

Structure and Defects in Sanidic Liquid Crystalline Polymers.

2. Structure Analysis of Sanidic Polymers by Simulation of Diffraction Patterns from Monomeric Analogs

I. G. Voigt-Martin,* P. Simon, D. Yan, and A. Yakimansky†

Institut für Physikalische Chemie der Universität Mainz, Jakob Welder Weg 11, 55099 Mainz, Germany

S. Bauer and H. Ringsdorf

Institut für Organische Chemie der Universität Mainz, Becher Weg 18-20, 55099 Mainz, Germany

Received May 2, 1994; Revised Manuscript Received July 22, 1994*

ABSTRACT: The diffraction patterns from sanidic polymers normally show 8–10 reflections of which only 4 or 5 are unique, so that it is impossible to solve their structure. A large number of equally probable models can easily be proposed. In this work, the monomeric analogs have been investigated by electron diffraction and imaging because they produce diffraction patterns which are rich in information and which can be analyzed to give the unit cell, its symmetry, and the direction of the molecule with respect to the cell axes. Clear analogies can be drawn with the spacings observed in the polymeric materials above the glass transition temperature.

1. Introduction

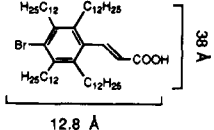
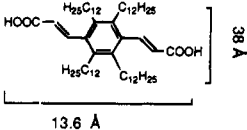
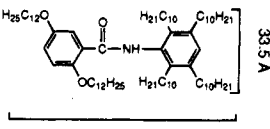
The structure of polymeric rodlike main chain polyesters/amides with long alkyl chains substituted as side groups has been a subject of debate for many years.^{1–4} The reason for the difficulty is the fact that these materials give rise to only 8–10 reflections, which is, of course, insufficient for structure analysis. The approach adopted in this paper is to crystallize the monomeric analogs of the polymers investigated in Part 1 and to determine their molecular structure. Electron diffraction was chosen because the crystals are much too small for X-ray analysis. The parameters obtained from the monomers are compared with those of the polymeric materials. Analogies are noted in order to obtain information about the structure of the polymer at a molecular level.

2. Samples Investigated and Why They Were Chosen

Stiff-chain aromatic polyesters and polyamides were originally synthesized with the aim of producing high-modulus fibers. Unfortunately, these materials cannot be processed because of their high melting temperatures and low solubilities. Therefore they were modified by the introduction of flexible side chains, thus reducing the transition temperature markedly. However, exploitation of the mechanical strength is only possible if the system is highly ordered. Many investigators have solved this problem in a pragmatic way by varying the molar mass and nature of the backbone, the length of the side chains, and the degrees of substitution, until materials which could be aligned were produced.

However, to optimize the desired properties, information about the mutual packing of these molecules is crucial. There is very little information available about this, despite the fact that numerous X-ray investigations have been undertaken. The reason for this is that

Table 1. Sanidic Half-Monomers

	Phase transition temperatures DSC measurements	Electron diffraction
<p>86</p> 	K ₁ 0 K ₂ 32 K ₃ 53 i	small angle: 24.1 Å wide angle: 5.0 Å
<p>77</p> 	K ₁ 86 K ₂ 148 i	small angle: 28.2 Å wide angle: 5.1 Å
<p>105</p> 	K 35 i	small angle: 25.6 Å wide angle: 5.0 Å

macroscopic samples are not well ordered, so that only powder or fiber diagrams can be obtained, giving relatively few unique reflections. These cannot, in principle, give sufficient information about the space group symmetry and can usually be simulated by many different model structures.

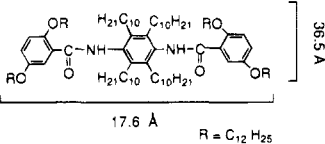
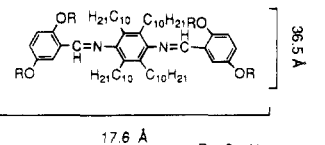
Therefore a different approach is undertaken in this work. Monomeric analogs of the polymers were synthesized, incorporating half, one, and one and a half monomeric units. The length and level of substitution correspond as closely as possible to those of the polymer.

The molecules are listed in Tables 1 and 2, together with their relevant lengths in the fully extended all-trans conformation. Samples 103 and 162 differ from each other only in the nature of the coupling between the phenylene rings. These samples were then crystal-

† Permanent address: Institute of Macromolecular Compounds, St. Petersburg, Russia.

* Abstract published in *Advance ACS Abstracts*, November 15, 1994.

Table 2. Comparison of Sanidic Oligomers

	Phase transition temperatures DSC	electron diffraction [010] zone (at 25°C)
103		
	K 105	small angle: 28.5 Å wide angle: 5.3 Å
162		
	K1, 75 K2, 95	small angle: 27.4 Å wide angle: 5.3 Å

lized. The crystals were too small for X-ray structural analysis and refinement; therefore electron diffraction and high-resolution imaging were used, requiring only microcrystals.

It is a fairly routine matter to deduce the unit cell, and consequently the lattice spacings, from diffraction patterns. However, the information which is needed to understand the physics at a molecular level is considerably more detailed than this; namely, we require the orientation and symmetry of the molecules in the unit cell and the mutual packing of the individual parts of the molecule. If this is understood, then the molecules can be precisely adapted to improve properties. Furthermore, the transition from crystal to liquid crystal can be better understood.

Structural research at a molecular level, which is referred to as structure refinement and which can now be performed routinely with direct methods in X-ray crystallography, is extremely difficult to perform in electron crystallography for reasons which are discussed in the text. However, by using the approach described in this paper, it has been possible to refine the structure of these highly substituted *p*-phenyleneterephthalamides.

3. Methods of Investigation

3.1. Electron Diffraction. Electron diffraction has become an increasingly important tool for structural investigations in recent years. The reason for this is that the following very powerful methods are now available, enabling electron diffraction to be used for structural analysis at atomic resolution.

1. *Direct Phase Methods.* These have been applied to the electron diffraction patterns of organic molecules to give potential maps with structural information at atomic resolution.^{5,6}

2. *Maximum Entropy Methods.* These use the Bricogne statistical approach, in which the a priori distribution of random atoms is updated by maximum entropy statistics. The phase information is induced from the observed intensities by using statistical methods from information theory. The information from real and reciprocal space is correlated by Fourier transformation and continually updated on statistical grounds.⁷⁻⁹

3. *Simulation of Experimental Diffraction Patterns.* The atomic coordinates of the molecule in the gas phase

can be obtained from semiempirical quantum mechanical methods using MOPAC 6.0. The molecule can then be placed into the unit cell determined from the electron diffraction pattern on the basis of the experimental *d*-spacings and symmetries. It is subsequently rotated and shifted using CERIUS, a program enabling on-line observation of the changing diffraction pattern as the molecule in the unit cell is adjusted. It is usually necessary to adjust the molecular conformation to obtain good agreement between experimental and simulated diffraction patterns and to avoid nonallowed close contacts between molecules. Finally, the calculated packing energy should be negative and the density about one.¹⁰⁻¹²

There are certain criteria which must be satisfied in order to use these methods. Both direct phase and maximum entropy methods require a large number of reliable intensities to begin the analysis procedure. We have shown in a number of papers recently that the maximum entropy approach is, in fact, very robust against individual inaccurate intensities,⁹ but in the present case there was an added difficulty: the samples were rather thick and certainly all the reflections were affected by dynamical scattering. Methods 1 and 2 therefore failed. In such cases it is better to try to achieve good qualitative agreement between experimental and simulated diffraction patterns. Their interpretation is difficult for the following reasons:

1. The measured intensities are unreliable because dynamical scattering affects individual reflections independently in a manner depending on sample thickness.¹¹⁻¹³

2. Radiation damage may destroy or alter the crystal structure before it can be recorded.¹⁴

3. Quantitative estimation of electron intensities is uncertain because correct background subtraction is difficult at small and large scattering angles.

However, in recent years we have been able to show that good structure analysis and refinement can be achieved by simulation, if diffraction patterns in several different projections are obtained.^{11,15} Moreover, dynamic effects can now be calculated.

3.1.1. Symmetry Considerations. The symmetry considerations are the most crucial part of the procedure and must be thoroughly understood before determining the space group and starting the simulation procedure.

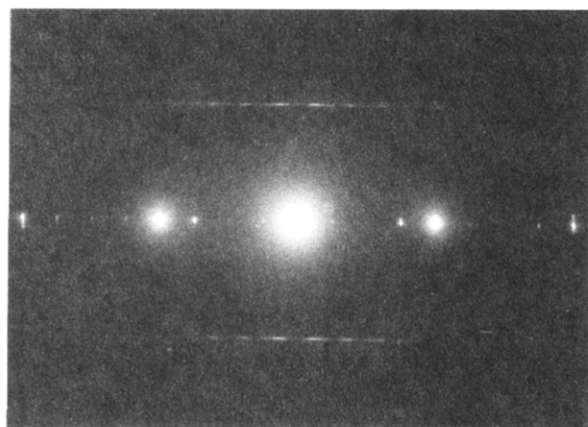
In a molecular crystal, the Fourier transform of the unit cell is a function of the transforms of the different molecules referred to their centers:

$$F_{\text{cell}}(q) = \sum_p \sum_j f_{pj}(q) \exp \{2\pi i [q(r_{jp} + r_p)]\} \quad (1)$$

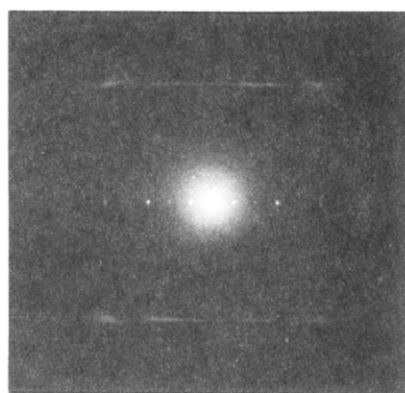
The summation *j* is extended over the atoms of each molecule and the summation over *p* to the centers of molecules.¹⁶

The diffraction amplitude of the unit cell content is derived in terms of the amplitudes diffracted by the different molecules of the unit cell. If the individual molecules are related by symmetry operations, there are specific relations between the corresponding transforms.

The electron diffraction patterns from different projections indicate, by its cell geometry and intensity relationships, the unit cell and possible space groups. The observed extinctions in different zones then reduce the number of possible space groups. The possible space groups must be determined before the simulation procedure can begin.



[100] zone (a)



[011] zone (b)

Figure 1. Experimental electron diffraction patterns of substituted *p*-phenyleneterephthalamide.

3.2. Powder X-ray Diffraction. X-ray powder diffraction patterns were obtained by standard methods using a Siemens D-500 diffractometer (Cu K α -radiation with a wavelength of $\lambda = 1.542$ Å) in a $\theta/2\theta$ X-ray reflectivity mode.

The single-crystal electron diffraction patterns are now indexed, so that the X-ray maxima in the same positions can also be given indices. If the unit cell is correct, consistent indexing can be achieved and, if necessary, an unknown parameter determined.

3.3. High-Resolution Imaging. The images which were obtained from the polymers in Part 1 showed that bent, highly distorted lattice planes were distributed in an amorphous matrix. Since organic samples are beam sensitive, it could be claimed that these features were a result of beam damage. Therefore it is important to compare the polymer images with those of the corresponding monomer crystals containing the same molecular segments.

High-resolution images were obtained by phase contrast imaging using low dose and cryo methods. The microscope transfer function was controlled by transferring the image via a videocamera to a computer with fast Fourier transform capabilities using the TIETZ VIPS system as described elsewhere.¹¹ We have shown previously that a very unorthodox transfer function must be used in order to transfer the spatial frequencies of interest for liquid crystals.^{13,14}

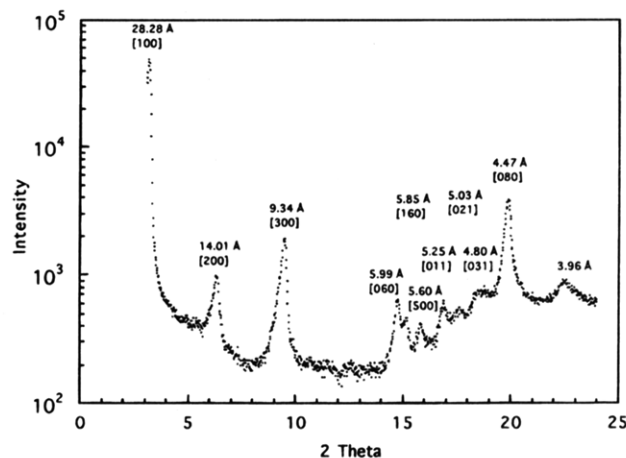


Figure 2. X-ray powder pattern of substituted *p*-phenyleneterephthalamide

Excellent images of defects can be made visible by this method.^{11–14} In crystals, additional, much smaller lattice spacings are to be expected; therefore, in principle, a different transfer function should be used to image these spacings. However, to compare the images from the polymer with those of the monomer, the same transfer function was chosen and therefore only the lattice planes corresponding to the small-angle spacings were imaged.

3.4. Computational Methods. 3.4.1. Calculation of Molecular Conformation. To calculate the molecular conformation, semiempirical quantum mechanical calculations were used.¹⁷ Although quantum chemists prefer ab initio methods, such efforts are not justified in this case (and for large molecules impossible) because the calculated gas-phase conformation will be changed by the crystal field. It is therefore only a first approximation in order to begin simulation. For this work, the results obtained by AM1 and PM3, which are incorporated in the MOPAC 6.0 package, were used.

Usually, several energy-minimized conformations are obtained. At this stage the symmetry requirements for crystal packing must be considered. The molecular symmetry must be chosen such that it relates to the symmetry group of the crystal (which was determined by the electron diffraction experiment). Therefore, symmetry considerations and energy minimization are the two criteria which are successively applied until a suitable conformation for the next simulation step is found.

3.4.2. Simulation of Electron Diffraction Pattern. The intensity and distribution of individual diffraction maxima depend on the Fourier transforms of the different molecules in the unit cell and their symmetry relationship to one another. The lattice parameters can be determined initially from the experimental diffraction pattern. By tilting or appropriate orientation of the crystal, the three lattice parameters and three angles between them are obtained from the experimental diffraction pattern. In addition to this, the space group is needed, which can be determined from the symmetry and related extinctions. The volume of the unit cell and the required density determine the number of molecules per unit cell. Together they must satisfy the symmetry requirements of the crystal. This imposes restrictions on the possible molecular conformation. Now the molecule is placed into the unit cell according to the required symmetry criteria and a diffraction pattern calculated. We have used CERIU for these investigations, as described previously.^{9,11,18}

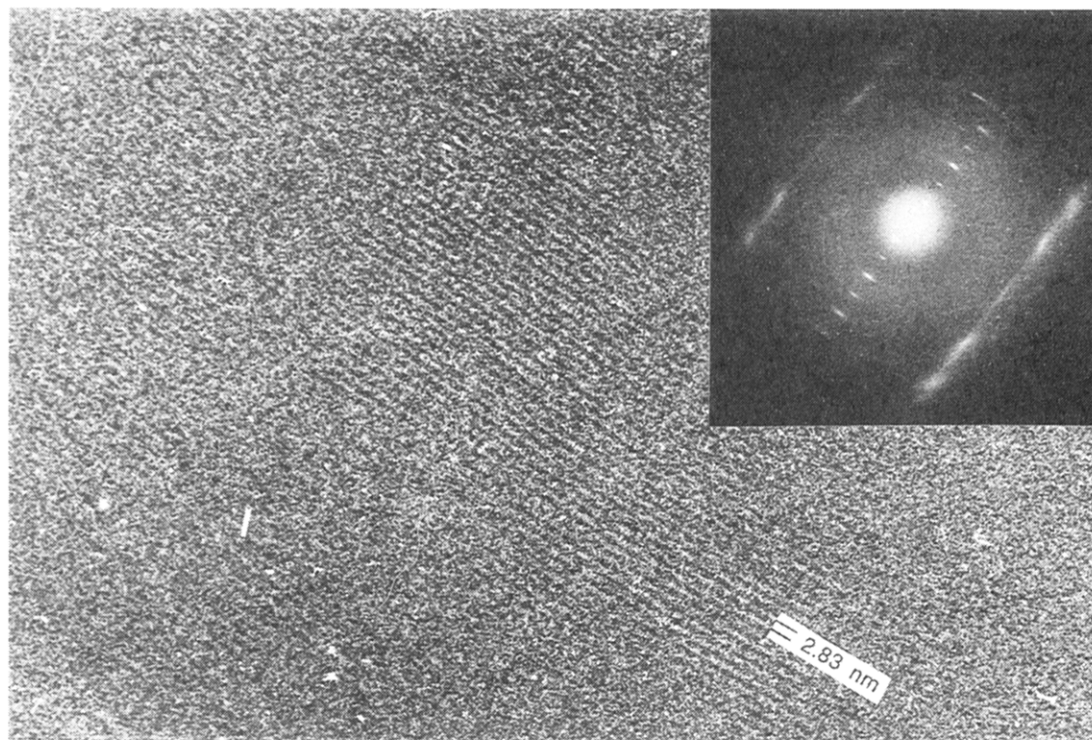


Figure 3. High-resolution image of substituted *p*-phenyleneterephthalamide with electron diffraction pattern.

Table 3. Conformational Angles of the Unsubstituted Main Chain of *N,N'*-(*p*-Phenylene)dibenzamide

method	angle ^a (deg)		
	ψ	ϕ	α
X-ray _{monoclinic} (ref 21)	29.1	35.9	65.0
X-ray _{orthorhombic} (ref 22)	22.7	56.3	79.0
force field (ref 23)	26.0	25.0	51.0

^a ψ = angle between the phenylenediamine segment and the amide plane; ϕ = torsional angle between the amide group and the benzoic acid unit; α = torsional angle between the outside phenylene rings (see also Figure 12).

Table 4. Conformational Angles of the Substituted Main Chain of *N,N'*-(*p*-Phenylene)dibenzamide

phase	angle ^a (deg)		
	ψ	ϕ	α
in gas phase/PM3	86.0	37.0	102.0
in crystal	85.9	44.7	94.0

^a ψ = angle between the phenylenediamine segment and the amide plane; ϕ = torsional angle between the amide group and the benzoic acid unit; α = torsional angle between the outside phenylene rings (see also Figure 12).

Table 5. Crystal Energy of Substituted Oligomeric Amide

van der Waals energy:	-206.7 kcal/mol
Coulomb:	+27.3 kcal/mol
H-bond:	-8.2 kcal/mol
total:	-187.5 kcal/mol

The molecule is then manipulated in the unit cell until good agreement is obtained between experimental and simulated diffraction patterns. This may involve adjustment of the conformation. If qualitatively good agreement in at least two zones can be achieved, the energy associated with this structure is calculated using the CERIUS Crystal Packer module. If the energy is not negative, the structure is discarded.

3.4.3. Simulation of X-ray Powder Pattern. The X-ray powder pattern was calculated for the structure previously determined by electron diffraction using CERIUS and compared with the experimental X-ray

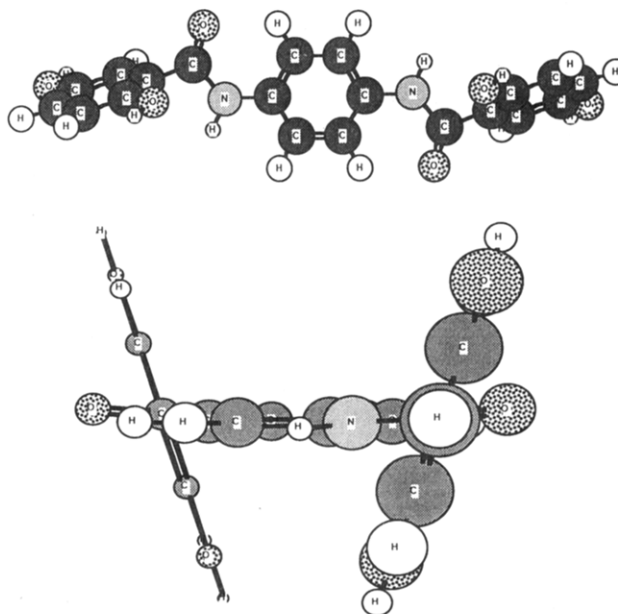


Figure 4. Minimum energy conformation of unsubstituted molecule in the gas phase from two different projections.

powder pattern. If the previous steps have been correctly performed, this is only a formality and should, of course, give good agreement between calculated and experimental patterns.

3.4.4. Simulation of Image. For image simulation the coordinates of all the atoms obtained in the previous sections are required and the image is calculated by double Fourier transformation, taking account of the imaging optics. To interpret the images obtained by phase contrast methods, it is essential to calculate the effect of the phase contrast transfer function and of sample thickness. The transfer function used experimentally was chosen such that spatial frequencies corresponding to the layers (20–30 Å) were transferred most efficiently. The images calculated by CERIUS are obtained in several steps by the classical reciprocal

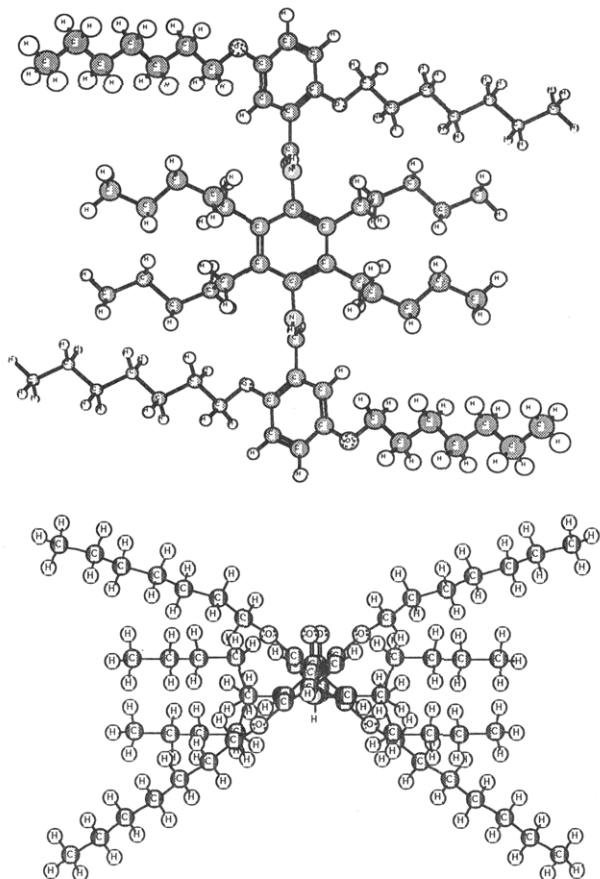


Figure 5. Minimum energy conformation of substituted molecule in the gas phase from two different projections.

space multislice approach:¹⁹⁻²⁰ (1) calculation of projected potential; (2) calculation of phase transmission function; (3) propagation of electron beam through crystal; (4) creating an image; (5) calculation of image intensity.

4. Results

4.1. Electron Diffraction. 4.1.1. Lattice Spacings. The lattice spacings determined for the crystalline monomeric analogs are listed in Table 1. A comparison with the results which were obtained from the corresponding polymers in the "sanidic phase" is obvious. The small-angle spacings between 25 and 28 Å and the wide-angle spacing of about 5 Å are identical to the distances observed in the polymers. These results offer additional evidence for the assumption that the material in region A of the DSC curves (Part 1) consists of poorly developed microcrystallites embedded in an amorphous matrix and that the sample only becomes truly liquid crystalline when a temperature corresponding to region C is attained.

Also indicated in Table 1 are the dimensions of the molecule. The same difficulty which was already observed for the polymers arises, namely, that the length of the molecule with fully extended side chains exceeds the long spacing by about 10 Å. In addition to this, the wide-angle spacing of 5 Å, also observed for the polymers, clearly corresponds to the distance between "boards" (see Figure 1a in Part 1). To propose a meaningful model structure, detailed analysis of the whole diffraction pattern obtained from different projections was undertaken for the amide 103.

4.1.2. Analysis of Electron Diffraction for a Specific Sample. Detailed analysis of the electron

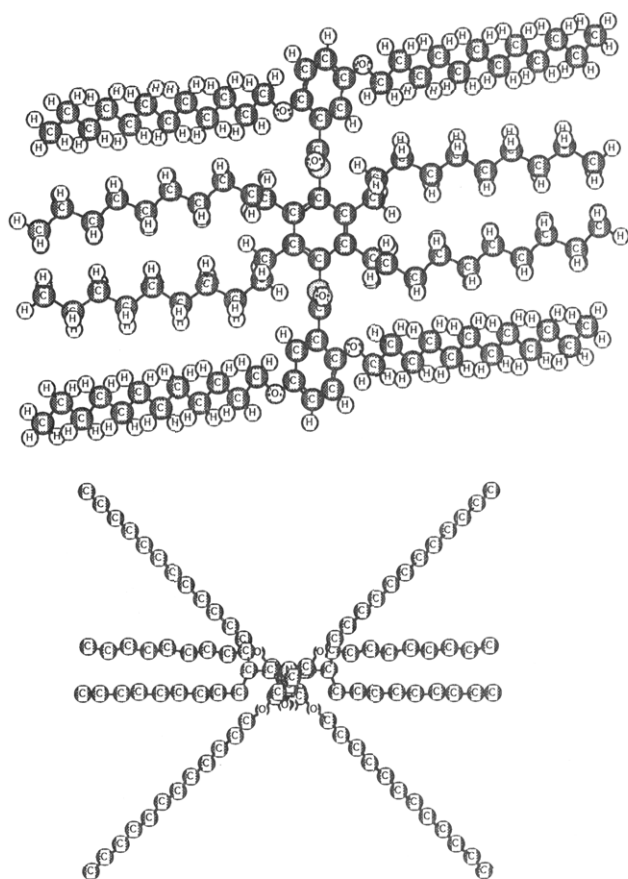
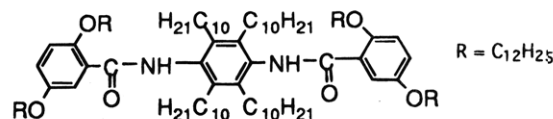


Figure 6. Molecular conformation of substituted molecule in the crystalline phase from two different projections.

diffraction pattern is demonstrated by a specific sample (103). Its chemical structure is shown below:



Different methods of preparation were used to obtain diffraction patterns from at least two zones. Solution growth and subsequent annealing in a magnetic field produced a [100] zone diffraction pattern (Figure 1a) whereas epitaxial growth on benzoic acid²¹ produced the [011] zone (Figure 1b). The diffraction patterns were indexed as shown.

From these experimental diffraction patterns the three basic axes were determined and shown to be perpendicular to one another. The observed extinctions in the experimental diffraction patterns are as follows: hkl , no conditions; $0kl$, $k + l = 2n$; $h0l$, $l = 2n$; $hk0$, no conditions; $h00$, no conditions; $0k0$, ($k = 2n$); $00l$, ($l = 2n$). The appropriate space group which satisfies these conditions is $Pnc2$. Therefore the result of electron diffraction suggests the following structure: $a = 28.2$ Å, $b = 35.9$ Å, $c = 5.28$ Å, $\alpha = 90^\circ$, $\beta = 90^\circ$, $\gamma = 90^\circ$, orthorhombic, space group $Pnc2$ 2 molecules/unit cell density 1.003 g/cm³.

For this space group there could be 4 molecules/cell in general positions or 2 molecules per cell in special positions ($1/2, 0, z$) and ($1/2, 1/2, 1/2 + z$). Since the density should be about 1 g/cm³, there must be 2 molecules per cell, in which case the molecule should have a two-fold axis. The observed extinctions permit the designation of two space groups, namely $Pnc2$ and

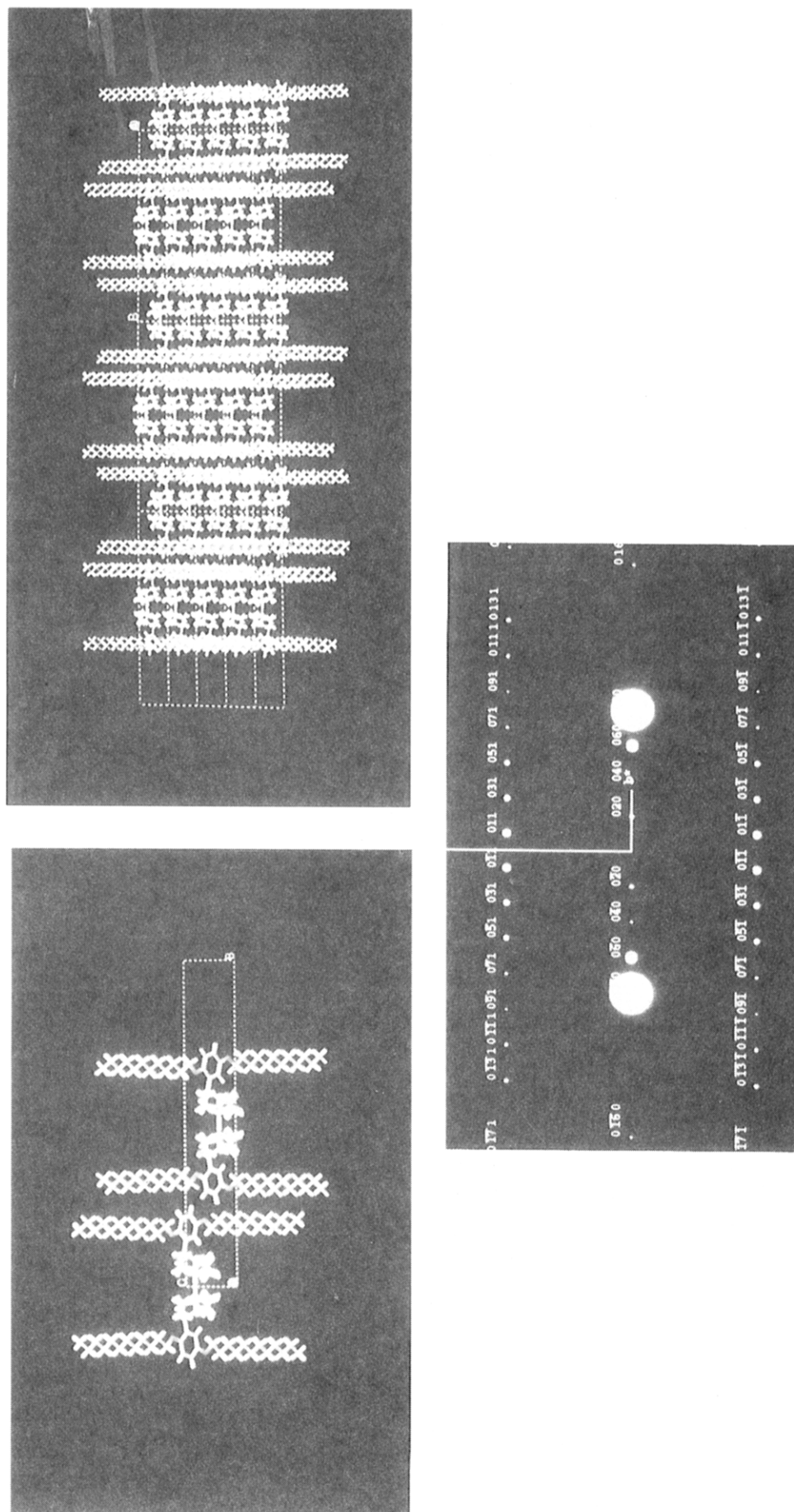


Figure 7. Simulated model in the b,c projection and corresponding [100] zone electron diffraction pattern.

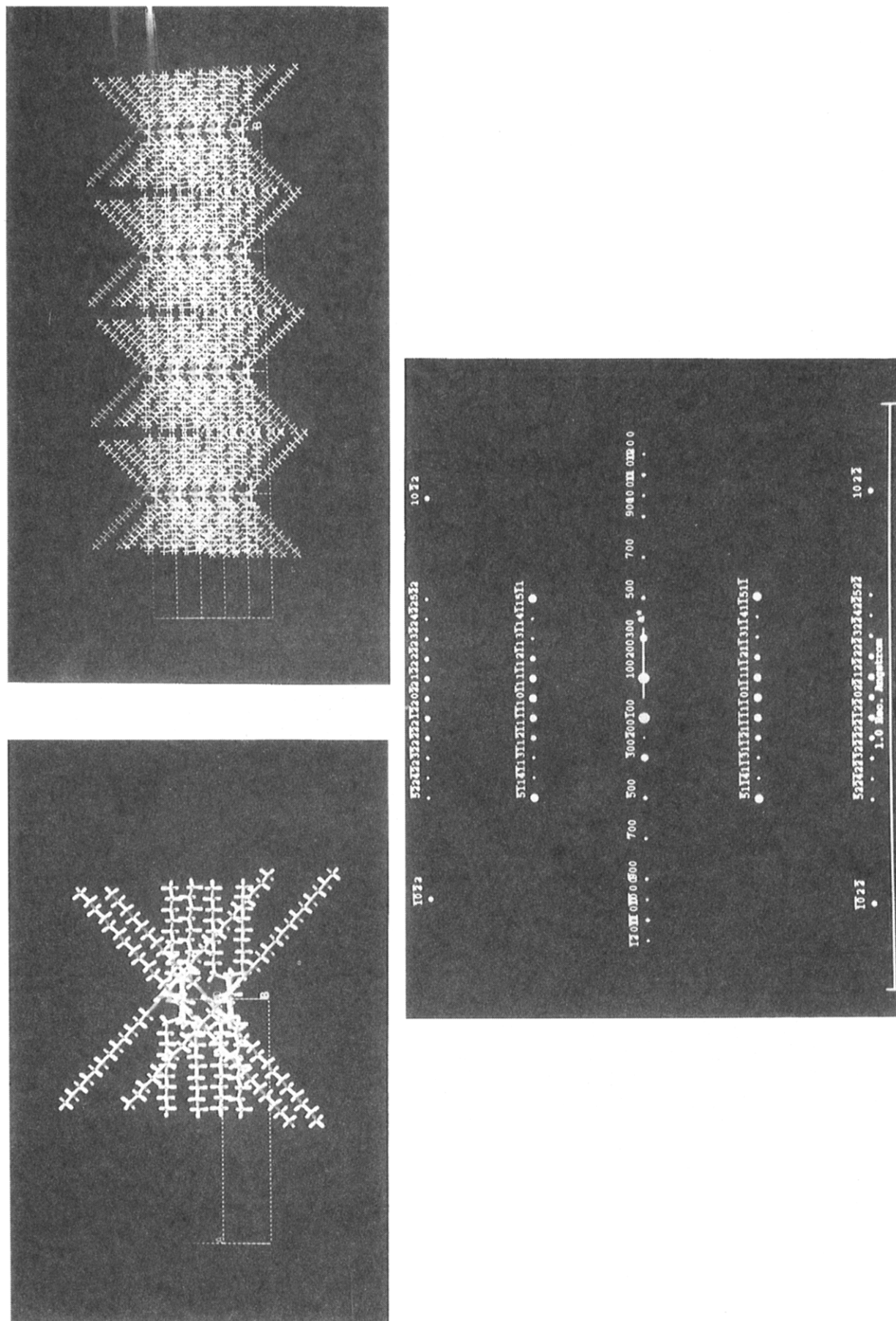


Figure 8. Simulated model and corresponding [011] zone electron diffraction pattern.

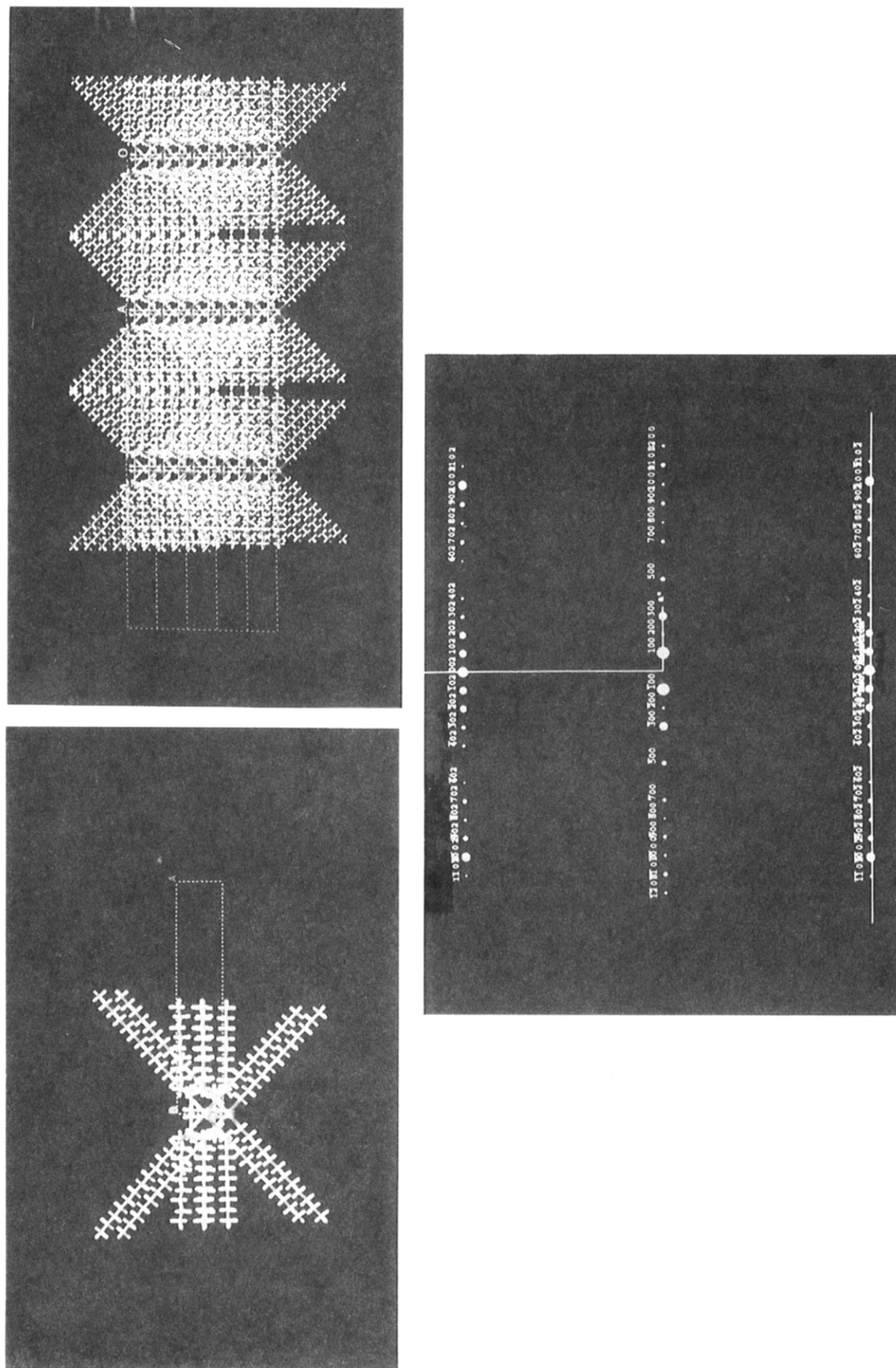


Figure 9. Simulated model in the a,c projection and corresponding [010] zone electron diffraction pattern.

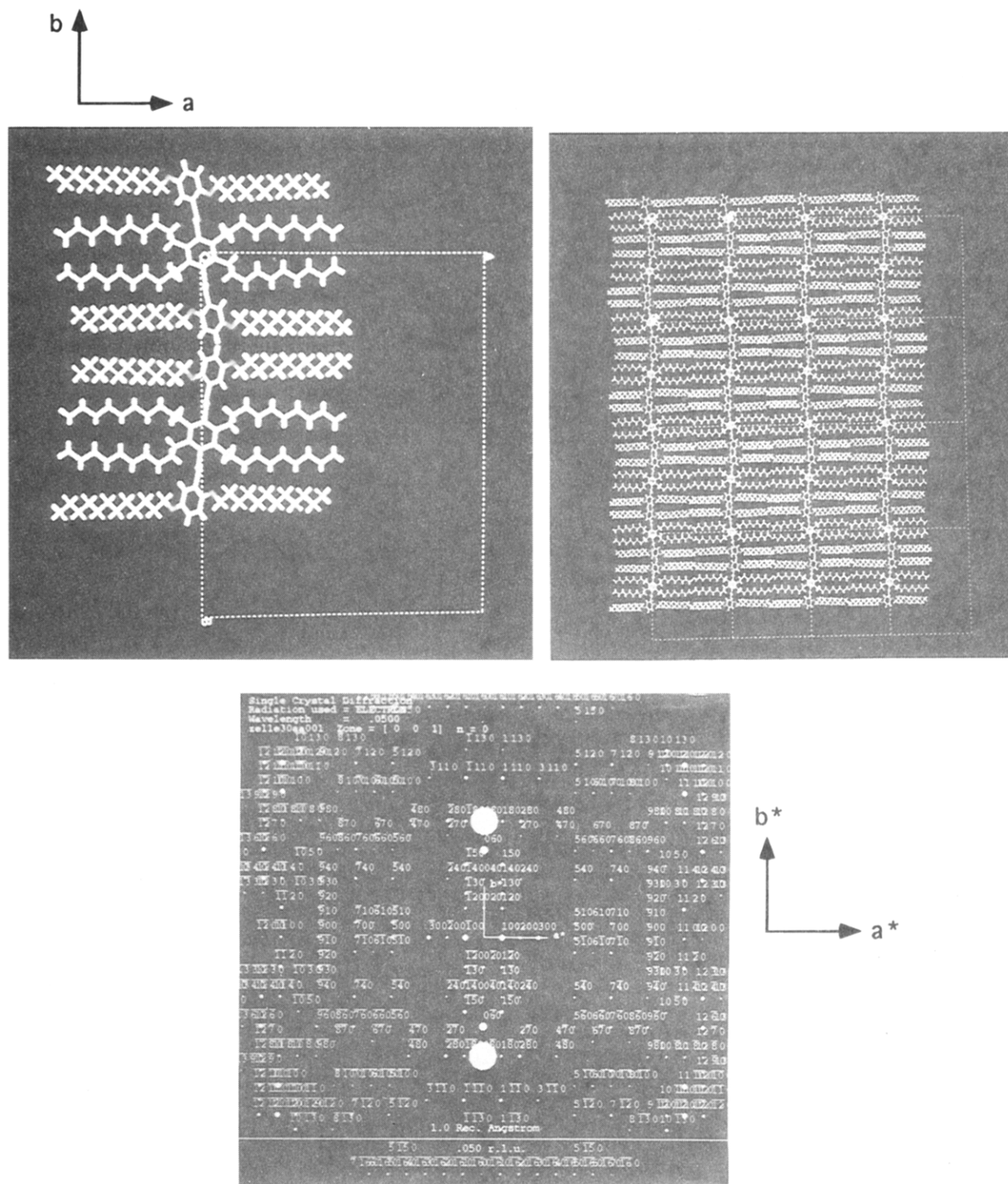


Figure 10. Simulated model in the a, b projection and corresponding [001] zone electron diffraction pattern.

Pnma. Choice of the former arose from packing considerations as described in section 4.4.2.

These considerations therefore deliver the information which is essential before the simulation procedure can begin; they represent the most crucial step in the whole analysis because they reduce the number of possible molecular conformations and the number of possible space groups.

The simulations will indicate whether the intensities of all the reflections correspond to the model proposed on the basis of these considerations.

4.2. X-ray Powder Method. The lattice spacings were confirmed by X-ray powder methods (Figure 2). The powder X-ray results can now be consistently indexed and confirm the (100), (200), and (300) reflections corresponding to the basic 28 Å repeat unit and

showing that there are no extinctions in the ($h00$) reflections. At the same time, only even ($0k0$) reflections are observed, with (080) being the strongest reflection. These observations confirm the a and b parameters determined by electron diffraction. In addition, the observed (011), (021), and (031) reflections confirm the c -axis and the angles $\alpha = \beta = \gamma = 90^\circ$. The systematic absences suggest a face-centered lattice, and the density requires 2 molecules per unit cell.

4.3. High-Resolution Images. The high-resolution images show that the lattice planes corresponding to the small-angle spacings are extremely long and straight, as is to be expected for a crystal (Figure 3). The high-resolution image confirms that the highly distorted lattice planes which were observed in the sanidic polymers (Part 1) are not caused by beam damage but

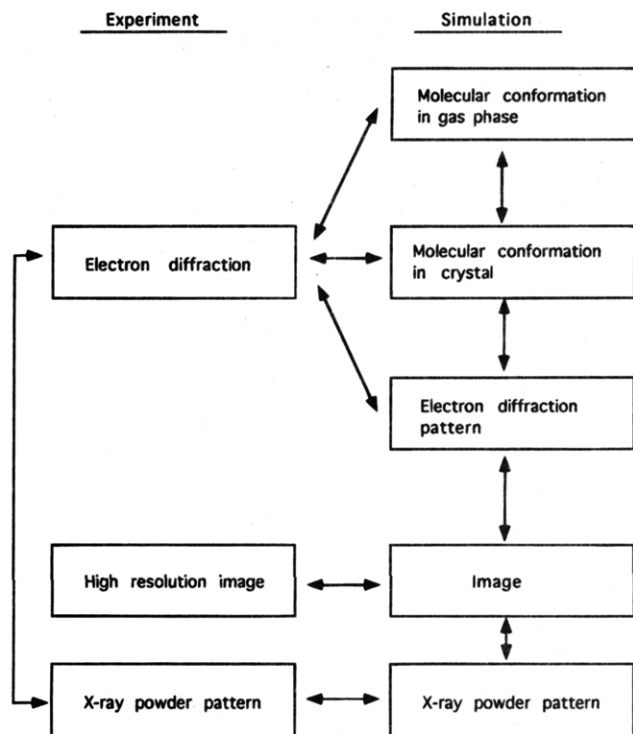


Figure 11. Flow diagram indicating analysis procedure.

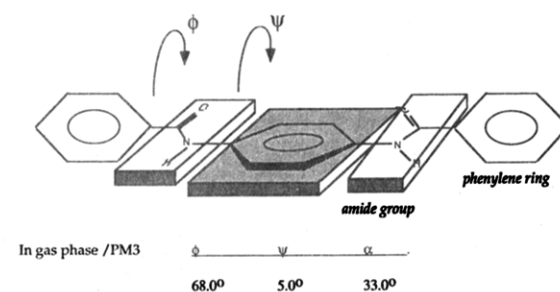
correctly represent the disturbed nature of the lattice planes.

4.4. Simulation of the Diffraction Pattern Obtained from Sample 103. **4.4.1. Molecular Conformation.** The structural formula of this molecule is shown in section 4.1.2. The molecular conformation for the unsubstituted main chain is well known from crystal structure analysis.^{22,23} In Table 3 and Figure 4, the relevant conformational angles of the unsubstituted main chain in the crystal are shown, as well as the results of force-field calculations.²⁴

Conformational calculations with the substituted main chain indicate an entirely different situation (Table 4 and Figure 5). The alkane chains attached to the phenylene cores produce a very strong intramolecular steric repulsion. The NH-CO unit is rotated further away from the plane of the phenylene core. In addition to this, each of the outer phenylene rings adopts an angle of 51° with respect to the central phenylene ring. The conformation in vacuum at 0 K calculated by MOPAC is shown in two different projections in Figure 5.

4.4.2. Simulation of Diffraction Pattern. The MOPAC-calculated molecule was placed into the experimentally determined unit cell using CERIUS, in such a manner as to obey the required symmetry and density conditions. The space group *Pnc2* with 2 molecules per unit cell requires that each molecule has a two fold axis. This two fold axis was placed in the crystallographic *c* direction. In this situation the CRYSTAL PACKER initially indicated a positive packing energy and a number of undesirable close contacts. Small adjustments were made to the molecule until the packing energy was negative and all close contacts avoided. The new conformation was checked against the experimental diffraction pattern. The final packing energy is shown in Table 5. Under these conditions, the calculated molecular conformation (Figure 6) shows only slight, but significant adjustments with respect to the minimum energy gas conformation (Figure 5). The alkane chains adopt an all-trans conformation and the

Unsubstituted molecule in gas phase



substituted molecule

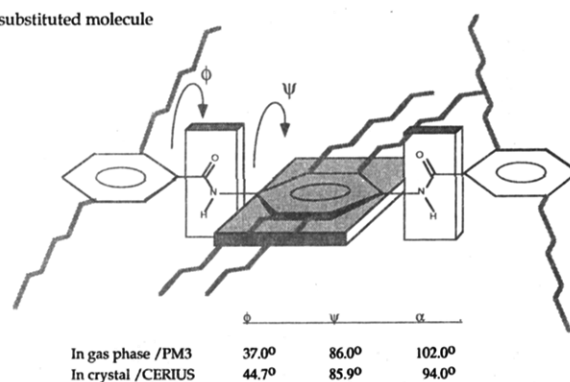


Figure 12. Conformation of *p*-phenyleneterephthalamide molecule. The angles ψ and ϕ denote torsional rotations of the amide group and phenylene ring with respect to the central core. α is the angle between the outside phenylene rings.

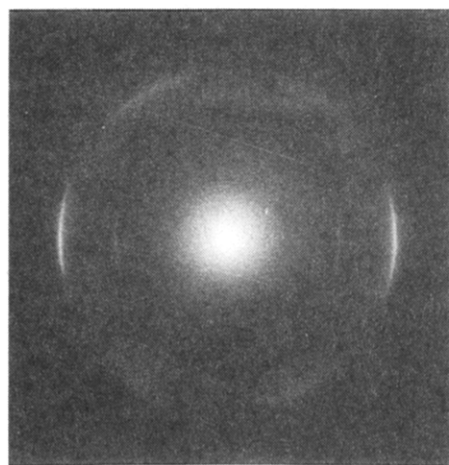
angle between the outer phenylene rings is reduced from 52 to 47°. Due to the tilt, the length of the molecule perpendicular to the main chain backbone is immediately reduced from 34.8 Å to the required 28.5 Å. Figures 7–10 show the major zones with corresponding molecular conformations and orientation in the unit cell. Comparison with the experimental diffraction patterns of Figure 1 immediately shows that the observed intensities correspond very well to the calculated [100] and [011] zones.

The calculated [001] zone corresponds well to the intensities observed in the polymer sample (Part 1). In this sample the strongest reflection in the b^* direction is the (080), corresponding to a distance of 4.2 Å between each of the 8 alkane chains in this direction. For the polymer this was the (060) reflection because that sample had 6 substituted alkane chains per corresponding segment of the main chain also with a distance of 4.2 Å between the alkane chains. The weaker (100), (200), and (300) reflections in the a^* direction correspond to the projected length of the TILTED alkane chains on the a, b projection in both cases.

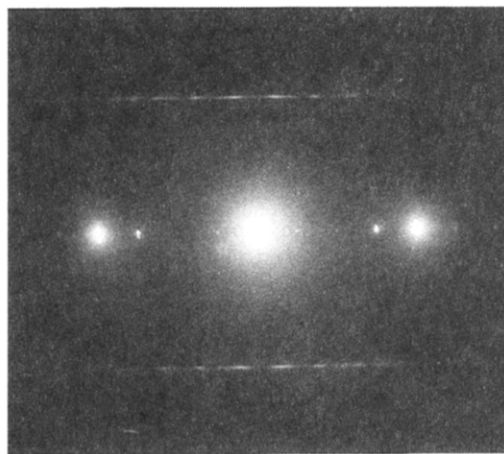
The decision between the space groups *Pnma* and *Pnc2* was difficult on the basis of extinctions alone. For *Pnma*, the molecules need a mirror plane or an inversion center. The mirror plane can be excluded because the molecule is not flat. An inversion center was still a possibility. However, this always produced a high packing energy and it was impossible to avoid nonallowed close contacts in the subsequent plane. The problem was easily avoided with a molecule having two-fold symmetry in a *Pnc2* space group, in which case a very low negative packing energy was achieved.

5. Summary

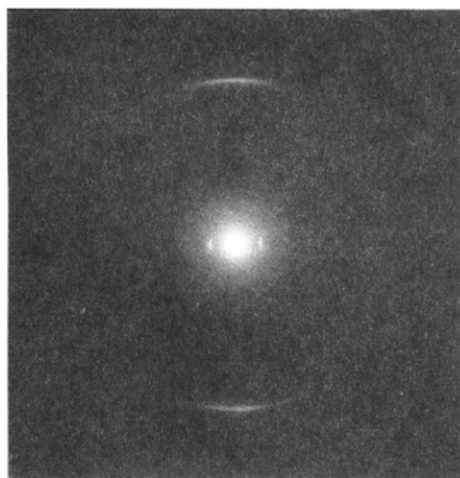
In this investigation an attempt has been made to solve the longstanding problem regarding the structure



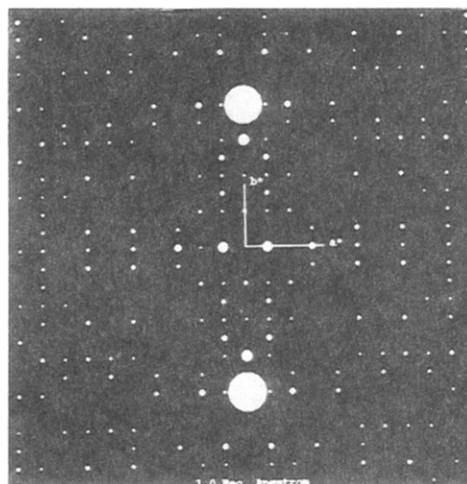
[100] zone polymer



[100] zone monomer



[001] zone polymer

[001] zone monomer
(simulated)**Figure 13.** Relationship between monomeric analog and polymer diffraction patterns (region A).

of biaxial "sanidic" polymers by using an entirely new approach. These samples always give rise to a biaxial diffraction pattern with some extraordinary features which are untypical for liquid crystals: (a) the small-angle reflections are broad; (b) higher-order reflections are stronger than lower-order reflections; (c) there are characteristic extinctions.

The number of available reflections is always too small for reliable structural analysis. Better orientation can be obtained by using monomeric analogs, but even these crystals are so small that X-ray structural analysis is impossible. Therefore selected-area electron diffraction was the only available route to success. This method cannot be used routinely, but we have demonstrated the success of a new approach, involving many steps as shown in the "flow diagram" (Figure 11). The results of this investigation can be summarized as follows:

(1) From the simulated diffraction patterns and their molecular models, it has been possible to calculate the molecular conformation in the crystalline phase and to show the precise changes in torsional angles arising due

to the crystal field. The results are summarized in Figure 12.

(2) The calculations from all zonal projections show excellent agreement with the experimental diffraction patterns. In particular, the models shown in detail how the alkane chain tilt accounts for the reduction in long spacing from 38 to 28 Å. This reduction is observed in both polymers (region A, Figure 9, Part 1) and monomers.

(3) The observed high intensities of higher-order reflections in both monomeric analogs and polymers (region A) arise from the lateral packing of alkane side chains. Observations 2 and 3 as well as the calculated [001] zone diffraction pattern show clearly that the biaxial diffraction pattern observed in the polymers in region A arises from microcrystallites with orientational disorder and with molecular conformations identical to those of the crystalline analogs. The relationship between monomeric analog and polymer diffraction patterns (region A) is shown in Figure 13.

(4) The high-resolution images in single crystals indicates long, straight lattice planes, as expected. In

contrast to this, in polymeric samples (region A) poorly developed crystallites are embedded in an amorphous matrix.

(5) The detailed investigation of molecular conformations in the crystalline phase shows the "boardlike" appearance in a,b projection with the a,c and b,c projections clearly show that the molecule is not flat due to rotation of the outer phenylene rings.

(6) The further reduction in long spacing on passing into the liquid crystalline phase can easily be understood by studying the a,b projection and corresponding [001] zone. Additional tilting between the outer phenylene rings reduces the a -axis still further, producing a new (100) reflection corresponding to 22 Å (Part 1, Figures 2 and 9, region C). At the same time, long-range correlations between alkane chains are lost, so that the strong $(080)_{\text{monomer}}/(060)_{\text{polymer}}$ reflection finally disappears.

(7) On passing into the liquid crystalline phase, columnar shift is possible along the b direction (Figure 10). However, because of the molecule conformation in the a,c direction (Figure 9), rotation of the molecules is impossible.

References and Notes

- (1) Ebert, M.; Herrmann-Schönherr, O.; Wenndorff, J. H.; Ringsdorf, H.; Tschirner, P. *Makromol. Chem., Rapid Commun.* **1988**, *9*, 451.
- (2) Ballauff, M.; Schmidt, G. F. *Macromol. Chem., Rapid Commun.* **1987**, *8*, 93.
- (3) Rodriguez-Parada, J. M.; Duran, R.; Wegner, G. *Macromolecules* **1989**, *22*, 2507.
- (4) Biswas, A.; Deutscher, K.; Blackwell, J.; Wegner, G. *Polym. Prepr. (Am. Chem. Soc., Div. Polym. Chem.)* **1992**, *33*, 286.
- (5) Dorset, D. *Biophys. J.* **1991**, *60*, 1366.
- (6) Dorset, D. *Ultramicroscopy* **1986**, *38*, 23.
- (7) Bricogne, G. *Acta Crystallogr.* **1988**, *A44*, 517.
- (8) Dong, W.; Baird, T.; Fryer, J. R.; Gilmore, C. J.; MacNicol, D. D.; Bricogne, G.; Smith, D. J.; O'Keefe, M. A.; Hovmöller, S. *Nature (London)* **1992**, *355*, 605.
- (9) Voigt-Martin, I. G.; Yan, D. H.; Gilmore, C. J.; Shankland, K. *Ultramicroscopy*, to be published.
- (10) Voigt-Martin, I. G.; Zhou, E.; Simon, P.; Garbella, R. W.; Yan, D.; Paulus, W.; Ringsdorf, H. *Adv. Mater. Optics Electronics* **1993**, *2*, 245.
- (11) Voigt-Martin, I. G.; Schumacher, M.; Garbella, R. W. *Macromolecules* **1992**, *25*, 961.
- (12) Voigt-Martin, I. G.; Schumacher, M.; Garbella, R. W. *Liq. Cryst.*, in press.
- (13) Voigt-Martin, I. G.; Krug, H.; Van Dyck, D. *J. Phys.* **1990**, *51*, 2347.
- (14) Voigt-Martin, I. G.; Durst, H. *Macromolecules* **1989**, *22*, 168.
- (15) Voigt-Martin, I. G.; Yan, D.; Wortman, R.; Elich, K. *Ultramicroscopy*, submitted.
- (16) Amoros, J. L.; Amoros, M. *Molecular Crystals: Their Transforms and Diffuse Scattering*; Wiley: New York, 1968.
- (17) Clark, T. A. *Handbook of Computational Chemistry*; Wiley: New York, 1985.
- (18) Voigt-Martin, I. G.; Schumacher, M.; Honig, M.; Simon, P.; Garbella, R. W. *Mol. Cryst. Liq. Cryst., Spec. Proc.*, 1993.
- (19) Cowley, J. M.; Moodie, A. F. *Acta Crystallogr.* **1959**, *12*, 353.
- (20) O'Keefe, M. A.; Buseck, P. R.; Spaego, A. E. C. *Ultramicroscopy* **1983**, *11*, 35.
- (21) Wittmann, J. C.; Hodge, A. M.; Lotz, B. *J. Polym. Sci., Polym. Phys. Ed.* **1983**, *21*, 2495.
- (22) Harkema, S.; Gaymans, R. J. *Acta Crystallogr.* **1977**, *B33*, 3609.
- (23) Adams, W. W.; Fratini, A. V.; Wiff, D. R. *Acta Crystallogr.* **1978**, *B34*, 954.
- (24) Hummel, J. P.; Flory, P. J. *Macromolecules* **1980**, *13*, 479.

MA940795S